An Alternating Method for Analysis of Surface-Flawed Aircraft Structural Components

T. Nishioka* and S. N. Atluri†
Georgia Institute of Technology, Atlanta, Georgia

A new alternating method for the analysis of a quarter-elliptical corner crack is developed. The completely general analytical solution for an embedded elliptical crack in an infinite solid, subject to arbitrary crack-face tractions, is implemented in the present alternating method. The present finite element alternating method results in an inexpensive procedure for the routine evaluation of accurate stress intensity factors for flawed structural components. The present alternating method is applied to the analyses of various shapes of quarter-elliptical corner cracks: 1) in a brick subject to remote tension, 2) emanating from a hole in finite-thickness plates subject to remote tension as well as bearing pressure; and 3) emanating from a pin hole in aircraft attachment lugs subject to simulated pin loading. The results for problems 1 and 2 are compared with those available in literature. for problem 3 the stress intensity factors and their parametric variations for the corner cracks of various shapes are presented.

Introduction

A KNOWLEDGE of accurate stress intensity factors is essential for a proper integrity analysis of flawed structures. Corner cracks at holes, such as in aircraft attachment lugs, have received much attention due to the fact that they are among the most common flaws in aircraft structural components. Analyses of corner cracks in aircraft attachment lugs are, needless to say, three-dimensional in nature; however, in most studies to date two-dimensional analyses have been employed, as in Refs. 1 and 2.

For the three-dimensional analyses of corner cracks at holes, Atluri and Kathiresan[3] used a hybrid three-dimensional crack element to directly evaluate the stress intensity factors along the crack border. Hechmer and Bloom[4] and Raju and Newman[5] used three-dimensional singularity wedge elements in which the stress intensity factors were indirectly extracted from computed results such as the nodal displacements or nodal forces. Smith and Kullgren[6] used a finite element alternating method in which the analytical solution for an elliptical crack in an infinite solid subject to a cubic pressure distribution[7] was used to obtain the stress intensity factors. Heliot, Labbens, and Pellissier-Tanon[8] used the boundary integral equation method. On the other hand, for the three-dimensional analyses of corner cracks in attachment lugs, very few solutions are available in literature.

A recent comprehensive study[9] revealed that although the "3-D hybrid crack element" method[3,10,11] yielded better accuracies than the alternating method,[12,13] the latter remained a potentially cheaper technique if it could be improved. One of the major impediments to obtaining accurate solutions through the alternating technique has been that the solution for an embedded elliptical crack in an infinite solid, which is the basic solution needed in the implementation of the alternating method, has been limited only to a cubic normal pressure variation on crack surface.[7]

Recently, a major improvement of the alternating technique has been made by the present authors.[14,15] In this new alternating method the complete, general analytical solution[15,16] for an embedded elliptical crack in an infinite solid, subject to arbitrary tractions (normal as well as shear) on the crack surface, was implemented in conjunction with the finite element method. It was demonstrated that the new finite element alternating method yielded accurate solutions of the stress intensity factors and is approximately one order of magnitude less expensive in computing costs as compared to those with the hybrid finite element method[3,10,11] and other techniques currently reported in literature.

In the present paper, using the new finite element alternating method, stress intensity factors are presented for quarter-elliptical corner cracks of various shapes: 1) in a finite-thickness plate (brick) subject to remote tension, 2) at the edge of a hole in finite-thickness plates subject to remote tension as well as bearing pressure loading, and 3) at the edge of a pin hole in aircraft attachment lugs subject to simulated pin loading. The present results for problems 1 and 2 are compared with other results available. For problem 3 the stress intensity factors and their parametric variations for the corner cracks of various shapes are presented.

Analytical Solution for an Elliptical Crack in an Infinite Solid with Arbitrary Crack-Face Tractions

In this section, only the mode I problem is considered. The complete, general solution including the modes II and III is given in Refs. 15 and 16. Suppose that x_1 and x_2 are Cartesian coordinates in the plane of the elliptical crack and x_3 is normal to the crack plane such that

$$(x_1/a_1)^2+(x_2/a_2)^2=1, \qquad a_1>a_2 \tag{1}$$

describes the border of the elliptical crack of aspect ratio (a_1/a_2). The elliptical coordinates ξ_α ($\alpha=1,2,3$) are defined as the roots of the cubic equation,

$$\omega(s)=1-\left(\frac{x_1^2}{a_1^2+s}\right)-\left(\frac{x_2^2}{a_2^2+s}\right)-\left(\frac{x_3^2}{a_3^2+s}\right)=0 \tag{2}$$

Let the normal traction along the crack surface be expressed in the form:

$$\sigma_{33}^{(0)}=\sum_{i=0}^{1}\sum_{j=0}^{1}\sum_{m=0}^{M}\sum_{n=0}^{m}A_{3,m-n,n}^{(i,j)}x_1^{2m-2n+i}x_2^{2n+j} \tag{3}$$

where the A are undetermined coefficients and the parameters

Presented as Paper 81-0497 at the AIAA/ASME/ASCE/AHS 22nd Structures, Structural Dynamics and Materials Conference, Atlanta, Ga., April 6-8, 1981; submitted Jan. 28, 1982; revision received July 19, 1982.

*Visiting Assistant Professor, Center for the Advancement of Computational Mechanics, School of Civil Engineering.

†Regents' Professor of Mechanics, Center for the Advancement of Computational Mechanics, School of Civil Engineering. Member AIAA.

i and j specify the symmetries of the load with respect to the axes of the ellipse, x_1 and x_2.

The solution corresponding to the load expressed by Eq. (3) can be assumed in terms of the potential function

$$f_3 = \sum_{i=0}^{1}\sum_{j=0}^{1}\sum_{k=0}^{M}\sum_{\ell=0}^{k} C_{3,k-\ell,\ell}^{(i,j)} F_{2k-2\ell+i,2\ell+j} \tag{4}$$

where

$$F_{2k-2\ell+i,2\ell+j} = \frac{\partial^{2k+i+j}}{\partial x_1^{2k-2\ell+i}\partial x_2^{2\ell+j}} \int_{\xi_3}^{\infty} [\omega(s)]^{2k+i+j+1} \frac{\mathrm{d}s}{\sqrt{Q(s)}} \tag{5}$$

and

$$Q(s) = s(s+a_1^2)(s+a_2^2) \tag{6}$$

and the C are also undetermined coefficients. The components of displacement u_i and stress σ_{ij} in terms of the derivatives of the potential functions (a comma followed by an index such as j implies partial differentiation with remaining term x_j) are given by

$$u_1 = (1-2\nu)f_{3,1} + x_3 f_{3,31} \tag{7a}$$

$$u_2 = (1-2\nu)f_{3,2} + x_3 f_{3,32} \tag{7b}$$

$$u_3 = -2(1-\nu)f_{3,3} + x_3 f_{3,33} \tag{7c}$$

and

$$\sigma_{11} = 2\mu(f_{3,11} + 2\nu f_{3,22} + x_3 f_{3,311}) \tag{8a}$$

$$\sigma_{22} = 2\mu(f_{3,22} + 2\nu f_{3,11} + x_3 f_{3,322}) \tag{8b}$$

$$\sigma_{12} = 2\mu(f_{3,12} - 2\nu f_{3,12} + x_3 f_{3,312}) \tag{8c}$$

$$\sigma_{33} = 2\mu(-f_{3,33} + x_3 f_{3,333}) \tag{8d}$$

$$\sigma_{31} = 2\mu x_3 f_{3,331} \tag{8e}$$

$$\sigma_{32} = 2\mu x_3 f_{3,332} \tag{8f}$$

where μ and ν are the shear modulus and Poisson's ratio, respectively. For later convenience, the stresses given by Eqs. (8) through Eqs. (4-6) are expressed in a matrix form,

$$\underset{6\times 1}{\{\sigma\}} = \underset{6\times N}{[P]}\ \underset{N\times 1}{\{C\}} \tag{9}$$

where $[P]$ is the function of the coordinates (x_1,x_2,x_3) and N is the total number of coefficients A or C.

Satisfying the boundary conditions on the crack surface, the relation between the coefficients A and C can be summarized in a matrix form

$$\underset{N\times 1}{\{A\}} = \underset{N\times N}{[B]}\ \underset{N\times 1}{\{C\}} \tag{10}$$

The detailed complete expression of components of $[B]$ is given in Ref. 15.

For a complete polynomial loading expressed by Eq. (3), the maximum degree of polynomial (*MXDOP*) and the total number of coefficients N can be expressed, respectively, by $MXDOP = 2M+1$ and $N=(M+1)(2M+3)3$. For an incomplete polynomial loading in which the symmetries of problem are accounted for, the maximum degree of polynomial and the number of coefficients depend on not only the parameter M but also the parameters i and j in Eqs. (3) and (4).

Once the coefficients C are determined by solving Eq. (10) for a given loading on the crack surface, the stress intensity factors corresponding to this load can be evaluated from the equation,[15,16]

$$K_I = 8\mu\left(\frac{\pi}{a_1 a_2}\right)^{1/2} A^{1/4} \sum_{i=0}^{1}\sum_{j=0}^{1}\sum_{k=0}^{M}\sum_{\ell=0}^{k}(-2)^{2k+i+j} \times (2k+i+j+1)!\frac{1}{a_1 a_2}\left(\frac{\cos\theta}{a_1}\right)^{2k-2\ell+i}\left(\frac{\sin\theta}{a_2}\right)^{2\ell+j} C_{3,k-\ell,\ell}^{(i,j)} \tag{11}$$

where θ is the elliptic angle measured from the x_1 axis, and

$$A = a_1^2\sin^2\theta + a_2^2\cos^2\theta \tag{12}$$

Finite Element Alternating Method

The alternating method for elliptical crack problem was originally developed by Shah and Kobayashi.[12,13] In their method, the solution for an elliptical crack, subject to a cubic polynomial pressure distribution in an infinite solid was implemented. Subsequently Smith et al.[6] introduced the finite element technique into the alternating method, employing the same solution[7] used by Shah and Kobayashi.[12,13] The limitation to a cubic polynomial pressure was one of the major impediments to obtaining accurate solutions through the alternating technique.

The present alternating method uses two basic solutions as follows:[14,15]

1) The complete, general analytical solution for an elliptical crack subject to arbitrary loadings on the crack surface, in an infinite solid, as explained in the previous section and in Ref. 15.

2) A general numerical solution technique such as the finite element method or the boundary element method.[25] In the present paper the finite element method is used to generate solution 2 because of its simplicity. Use of a finite element method enables the alternating method to be applied to more complex structural components.

The steps required in the present alternating method are explained as follows (also see Fig. 1):

1) Solve the uncracked body under the given external loads by using the finite element method. The uncracked body has the same geometry as the given problem except for the crack. To save computational time in solving the finite element equations repeatedly, an efficient equations solver OPTBLOK[17] which has a resolution facility was implemented as explained in Ref. 15. In OPTBLOK, the reduction of the stiffness matrix is done only once, although the reduction of load vector and back substitution may be repeated for any number of iterations with only a small additional computational time.

2) Using the finite element solution, we compute the stresses at the location of original crack in the uncracked solid.

3) Compare the residual stresses calculated in step 2 with a permissible stress magnitude. Usually the permissible stress magnitude is chosen as 1% of the maximum external applied stress.

Alternatively the convergency of the analysis is also checked with a norm of stress intensity factor,

$$\|K_I\| = \sum_{\ell=1}^{L} |K_I(\theta_\ell)|/L \tag{13}$$

in which L points are chosen along the crack front. The change in the norm of stress intensity factor for each cycle of iteration is also monitored. For most cases, the change in the norm between the second and third iterations becomes less than 1%.

4) To satisfy the stress boundary condition on the crack surface, reverse the residual stresses. Then determine the coefficients A in Eq. (3) for the applied stress on the crack surface, by using the following least square fitting,

$$I=\int_{S_c}(\sigma_{33}^R-\sigma_{33}^{(0)})^2\mathrm{d}S \tag{14}$$

where σ_{33}^R is the reversed residual stress calculated by the finite element method, S_c the region of the crack, and I the functional to be minimized. The more detailed procedure in this step is given in Ref. 15.

5) Determine the coefficients C in Eq. (4) for the potential function by solving Eq. (10), ($\{C\}=[B]^{-1}\{A\}$).

6) Calculate the stress intensity factor for the current iteration by substituting coefficients C in Eq. (11).

7) Calculate the residual stresses on external surfaces of the body due to the applied stress on the crack surface in step 4. To satisfy the stress boundary condition on the external surfaces of the body, reverse the residual stresses and calculate equivalent nodal forces. These nodal forces $\{Q\}$ can be expressed in terms of the coefficients C,

$$\{Q\}_m=-\int_{S_m}[N]^T[n]\{\sigma\}\mathrm{d}S=[G]_m\{C\} \tag{15}$$

$$[G]_m=\int_{S_m}[N]^T[n][P]\mathrm{d}S \tag{16}$$

where $[N]$ is the matrix of isoparametric element shape function, $[n]$ the matrix of the normal direction cosines, and $[P]$ the basis function matrix for stresses and defined in Eq. (9). In order to save computational time, the matrices $[G]_m$ are calculated prior to the start of iteration process shown in Fig. 1. Although the matrix $[P]$ has the singularity of order $1/\sqrt{r}$ at the crack front, the magnitude of the matrix $[P]$ (or stress) decays rapidly with the distance from the crack front. Thus, the matrices $[G]_m$ are calculated only at the surface elements which satisfy the following condition:

$$r_{\min}<5a_1 \tag{17}$$

where $r_{\min}$ is the distance of the closest nodal point of each surface element from the center of the elliptical crack as shown in Fig. 2.

8) Consider the nodal forces in step 7 as externally applied loads acting on the uncracked body. Repeat all steps in the iteration process until the residual stresses on the crack surface become negligible (step 3). To obtain the final solution, add the stress intensity factors of all iterations.

Since the analytical solution for an elliptical crack in an infinite solid is implemented as solution 1, it is necessary to define the residual stresses over the entire crack plane, including the fictitious portion of the crack which lies outside of the finite body. Moreover, it is well known that the accuracy of the least squares fitting inside of the fitting region can be increased with the increasing number of polynomial terms; however, the fitting curve may change drastically in the region outside of the fitting. For these reasons, in Ref. 15 numerical experimentation was done to arrive at an optimum pressure distribution on the crack surface extended into the fictitious region. For a semielliptical crack which lies in the region of $-a_1\le x_1\le a_1$ and $0\le x_2\le a_2$, it was concluded that the fictitious pressure which, for the region of $-a_2\le x_2\le 0$, remains constant in the x_2 direction but varies in the x_1 direction gives the best result among the several numerical

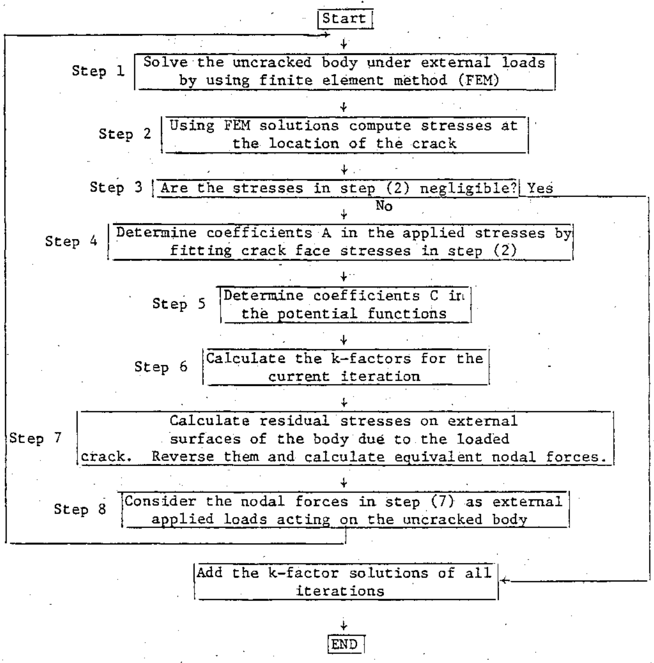

Fig. 1 Flow chart for finite element alternating technique.

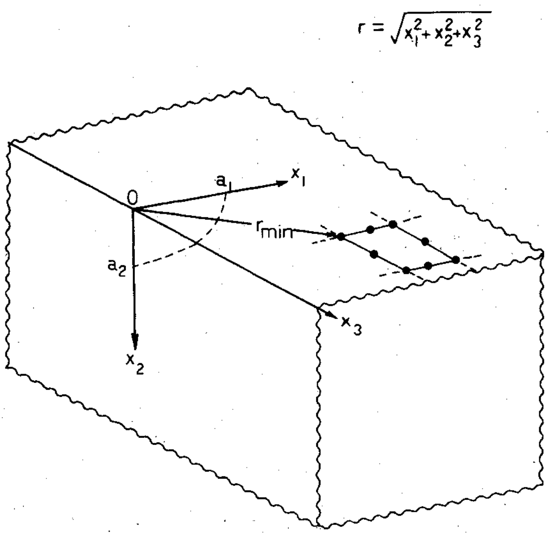

Fig. 2 Quarter-elliptical crack and distance of surface element.

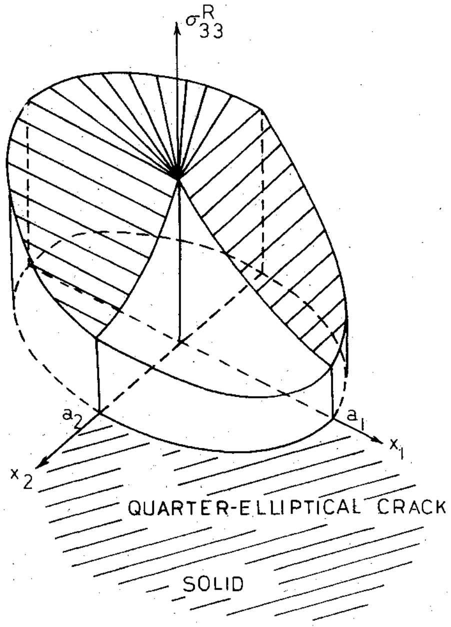

Fig. 3 Residual stress distribution over the entire crack surface.

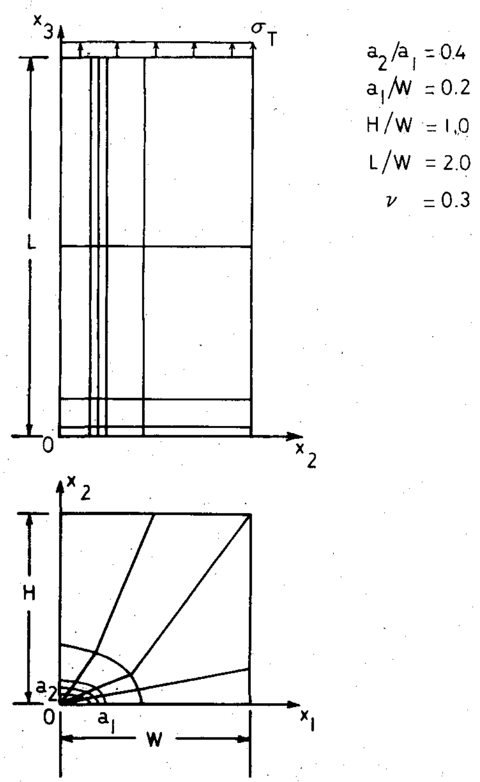

Fig. 4 Finite-element breakdown for an uncracked brick.

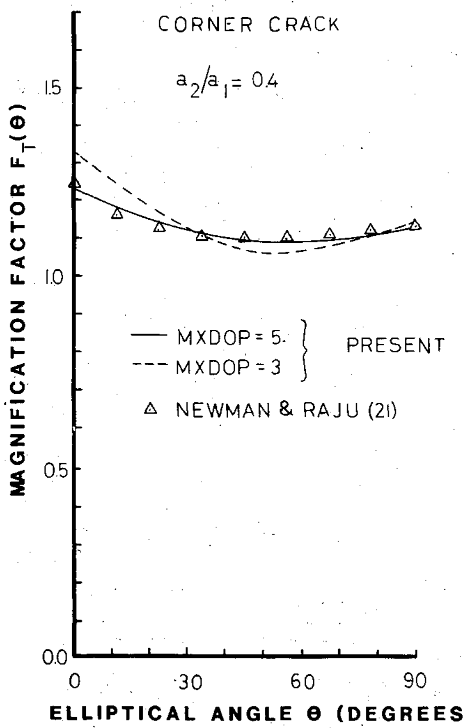

Fig. 5 Magnification factors for a quarter-elliptical corner crack in a brick.

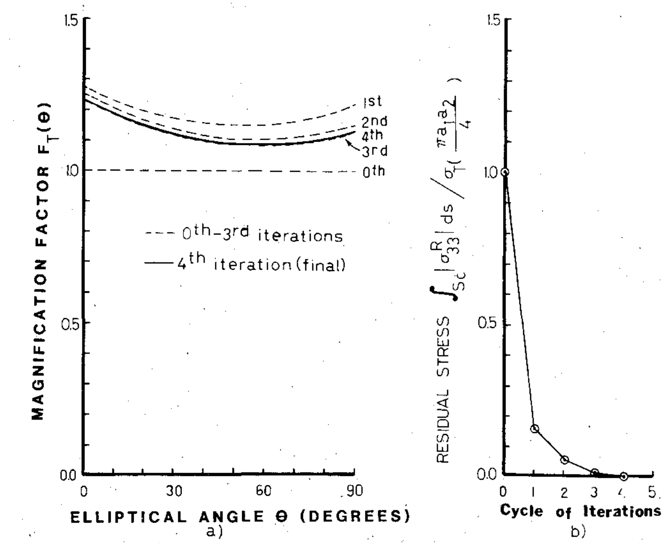

Fig. 6 Convergency of the solution obtained by the alternating technique, *MXDOP* = 5: a) succesive iteration for stress intensity factor, and b) variation of residual stress on the crack surface.

experiments performed in Ref. 15. The procedure of the fictitious pressure distribution for a semielliptical surface crack was successfully used in the analyses of surface cracks, in finite thickness plates subject to remote tension as well as remote bending,[15] and in pressure vessels.[18]

In the present paper, taking account of the conclusion drawn in Ref. 15 the fictitious pressure distribution shown in Fig. 3 is employed for the analysis of a quarter-elliptical corner crack. For the first quadrant $(x_1, x_2 \geq 0)$, the residual stress can be calculated by the finite element method and is a function of the coordinates x_1 and x_2. For the other quadrants, the fictitious residual stress is defined as

$$\begin{aligned} \sigma_{33}^R &= \sigma_{33}^R(0,x_2) \quad \text{for the second quadrant} \quad (x_1 \leq 0, x_2 \geq 0) \\ &= \sigma_{33}^R(0,0) \quad \text{for the third quadrant} \quad (x_1, x_2 \leq 0) \\ &= \sigma_{33}^R(x_1,0) \quad \text{for the fourth quadrant} \quad (x_1 \geq 0, x_2 \leq 0) \quad (18) \end{aligned}$$

Results and Discussions

Twenty-noded isoparametric elements were used in the present study. In the previous studies[14,15,18] the $3 \times 3 \times 3$ product Gauss integration rule was used to evaluate the stiffness matrices of the 20 noded isoparametric elements. In the present study the product Gauss integration rule was replaced by the 14 points nonproduct rule for three-dimensional integration.[19,20] All numerical analyses were performed by using the CDC CYBER 74 at Georgia Institute of Technology.

All problems considered here concern the linear elastic mode I problems of quarter-elliptical corner cracks. To quantify the effects of a finite body, crack aspect ratio, etc., a magnification factor (normalized stress intensity factor) F_i defined by the following equation is used,

$$F_i(\theta) = K_I(\theta) \Big/ \left(\frac{\sigma_i}{E(k)} \sqrt{\frac{\pi a_2}{a_1}} A^{1/4} \right) \quad (19)$$

where σ_i is a reference stress magnitude, $E(k)$ is the complete elliptic integral of second kind, $k^2 = (a_1^2 - a_2^2)/a_1^2$, and A is defined by Eq. (12). The denominator of the right side of Eq. (19) corresponds to the exact stress intensity factor for the elliptical crack subject to the constant pressure σ_i on the crack surface in an infinite solid. The reference stress σ_i depends on the type of problem considered.

Quarter-Elliptical Corner Crack in a Brick

We consider a brick containing a quarter-elliptical corner crack of aspect ratio $a_2/a_1 = 0.4$ and subject to remote tension σ_T at the ends of the brick. The geometries of this problem and the finite element breakdown for the uncracked brick are shown in Fig. 4. Due to the symmetry with respect to the x_3 direction, only the upper half of the brick was modeled by finite elements. It should be noted that the finite element method is used to analyze the uncracked body, although the mesh pattern follows the original crack shape. Thus, all the

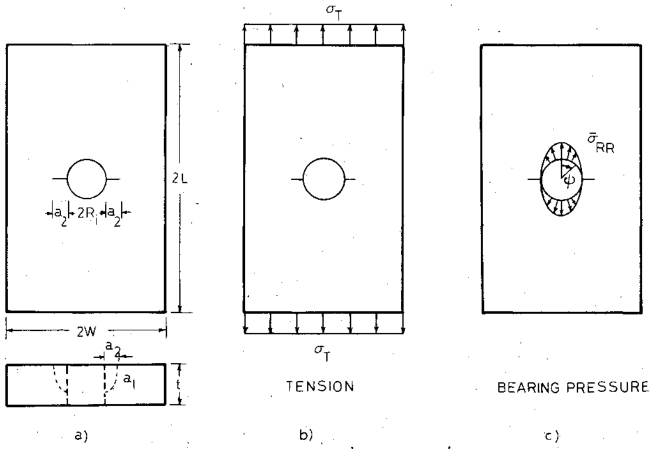

Fig. 7 Two symmetric quarter-elliptical corner cracks emanating from a hole in a finite-thickness plate: a) plate configuration, b) remote tension, and c) bearing pressure loading.

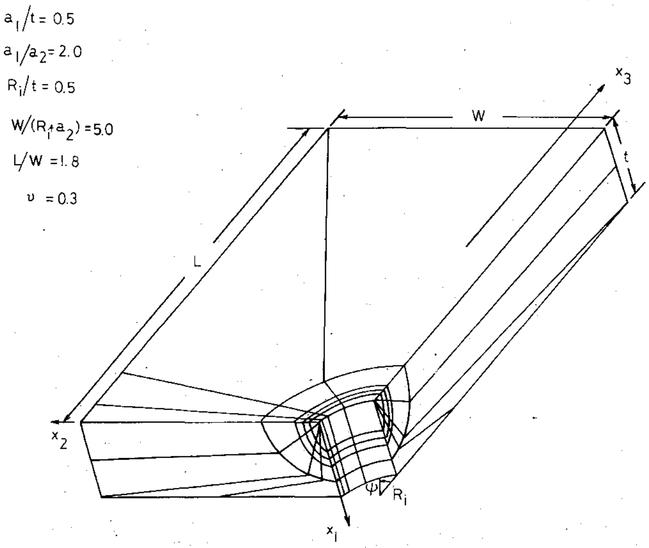

Fig. 8 Finite element breakdown for the uncracked plate with a hole.

displacements u_3 on the plane of $x_3=0$ are constrained due to the symmetry. The finite element mesh shown in Fig. 4 consists of 80 twenty-noded isoparametric elements with 1377 degrees of freedom (before imposition of the boundary conditions). The matrices $[G]_m$ given in Eq. (16) are calculated on the surface elements of $x_1=0$ and $x_2=0$ satisfying the condition of Eq. (17), $r_{\min} < 5a_1$, prior to the start of iteration process. It is noted that all surface elements on $x_1=W$, $x_2=H$, and $x_3=L$ are excluded in the calculation of $[G]_m$, since these boundaries are far enough from the crack.

The variation of the magnification factor F_T (normalized stress intensity factor) is shown in Fig. 5. The magnification factors were evaluated by using Eq. (19) with the reference stress $\sigma_i=\sigma_T$. In this case the value $E(k)=1.1507$ was used for $a_2/a_1=0.4$. In the present analysis 21 terms of the fifth-order polynomial ($MXDOP=5$: $M=2$, $i=0,1$; $j=0,1$) in Eq. (3) were used for the fitting of the residual stress in step 4. Figure 5 also shows the result with the cubic polynomial fitting ($MXDOP=3$: $M=1$; $i=0,1$; $j=0,1$). The present results are compared with the results from Newman and Raju.[21] As seen from the figure the present result with $MXDOP=5$ is in excellent agreement with those of Newman and Raju,[21] while the result with $MXDOP=3$ differs.

The stress intensity factor variation after each iteration and the residual stress removed from the crack surface in each iteration are shown for $MXDOP=5$ in Figs. 6a and 6b, respectively. As seen from the figures, the increment of the magnification factor for each iteration correlates with the residual stress removed from the crack surface. The magnitude of residual stress decreases monotonically with the increasing number of iterations. The increment of the norm for stress intensity factor variation defined by Eq. (13) for the fourth iteration (final) was only 0.2%. The CPU time for this analysis was 990 s using the CYBER 74.

Quarter-Elliptical Corner Cracks Emanating from a Hole in Finite-Thickness Plates

The configuration of the specimen considered here is shown in Fig. 7. Two symmetrical quarter-elliptical corner cracks emanating from the hole are considered. The definition of the

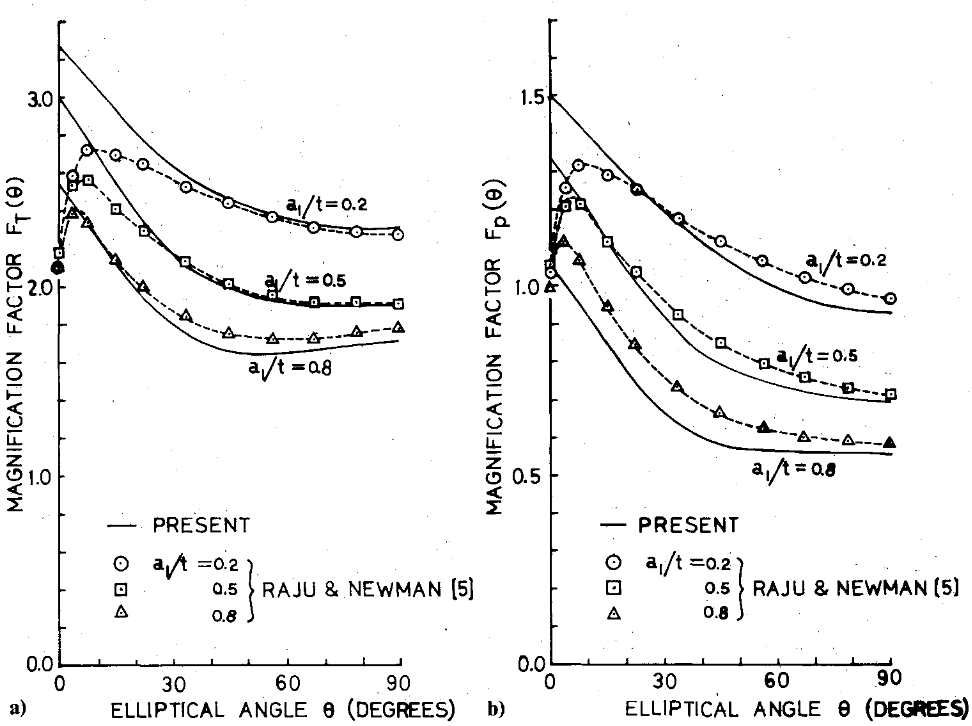

Fig. 9 Magnification factors for two symmetric quarter-elliptical corner cracks emanating from a hole in a plate: a) remote tension, and b) bearing pressure loading.

problem is identical to that in Ref. 5. The geometries for this problem are summarized as follows

$$a_l/a_2=2.0, \quad a_l/t=0.2,\ 0.5,\ \text{and}\ 0.8$$

$$R_i/t=0.5, \quad W/(R_i+a_2)=5.0, \quad L/W=1.8$$

For each crack geometry, two separate loadings were applied to the plate as shown in Figs. 7b and 7c. The applied normal stress $\bar{\sigma}_{RR}$ on the hole boundary in Fig. 7c is given by

$$\bar{\sigma}_{RR}=-(3P/4R_it)\cos^2\psi \tag{20}$$

where P is the total force acting on the perpendicular direction to the crack plane. It is noted that the origin of polar coordinates (R,ψ) is located at the center of the hole.

The typical finite element model used for the uncracked plate with a hole is shown in Fig. 8, which consists of 80 finite elements with 1377 degrees of freedom (before imposition of boundary condition). Due to the symmetries, only one-quarter of the plate was used in the analysis. The matrices $[G]_m$ are calculated on the surface elements of $x_l=0,t$ and $R=R_i$, satisfying Eq. (17), $r_{\min}<5a_l$, prior to the start of iteration process. The surfaces of $x_2=W-R_i$, $x_3=L$ can be excluded in the calculation of $[G]_m$ since these surfaces are far enough, i.e., $r_{\min}\geq 5a_l$. Since the global stiffness matrix and the matrices $[G]_m$ are the same, the two types of loading shown in Figs. 7b and 7c are solved at once for each crack geometry. Thus, as explained earlier, the reduction of stiffness matrix was made only once, while the reduction of the load vector and the back substitution were repeated for the two loading cases as well as for the iteration process in the alternating technique. The CPU time for each crack geometry with two loading cases was approximately 1200 s using the CYBER 74.

The magnification factors for remote tension and bearing pressure loading are shown in Figs. 9a and 9b, respectively. To evaluate the magnification factors the reference stress was chosen as $\sigma_i=\sigma_T$ for remote tension and $\sigma_i=\sigma_P\equiv P/2R_it$ for bearing pressure loading. The complete elliptic integral of second kind in Eq. (20) is equal to 1.211 for $a_l/a_2=2.0$. The present results are compared with those obtained by Raju and Newman.[5] For both the remote tension and bearing pressure cases, the present results are in excellent agreement with those from Ref. 5 except near the hole surface ($\theta=0$). It should be remarked that the comparison results of Raju and Newman[5] for the bearing pressure case shown in the present Fig. 9b are substantially different from those shown in Fig. 8b of the authors' original paper.[22] It was found there (Fig. 8b of Ref. 22) that the results of Ref. 5 differed significantly from the present ones in the bearing pressure case for the geometries $(a_l/t)=0.2$ and 0.5. However, a subsequent communication from Newman[23] indicated that the cited results in Ref. 5 were incorrect due to a computer input error. Thus, the corrected results[23] are in excellent agreement with the present results as shown in Fig. 9b.

The effect of the variation of bearing pressure is also examined. Another type of pressure distribution is given by

$$\bar{\sigma}_{RR}=-[2P/(\pi R_it)]\cos\psi \tag{21}$$

This cosine pressure loading gives a higher stress concentration factor as compared to that obtained from the cosine square loading given by Eq. (20). The magnification factors for both the pressure loadings are compared in Fig. 10. As can be expected from the elasticity solutions,[22] the magnification factor for the cosine pressure loading is slightly higher at the hole surface ($\theta=0$) and slightly lower at the plate surface ($\theta=\pi/2$) than that from cosine square loading.

The present results shown in Fig. 9 were obtained for two symmetric quarter-elliptical corner cracks. The stress intensity factor for a single quarter-elliptical corner crack can be converted from the results for two symmetric cracks by using

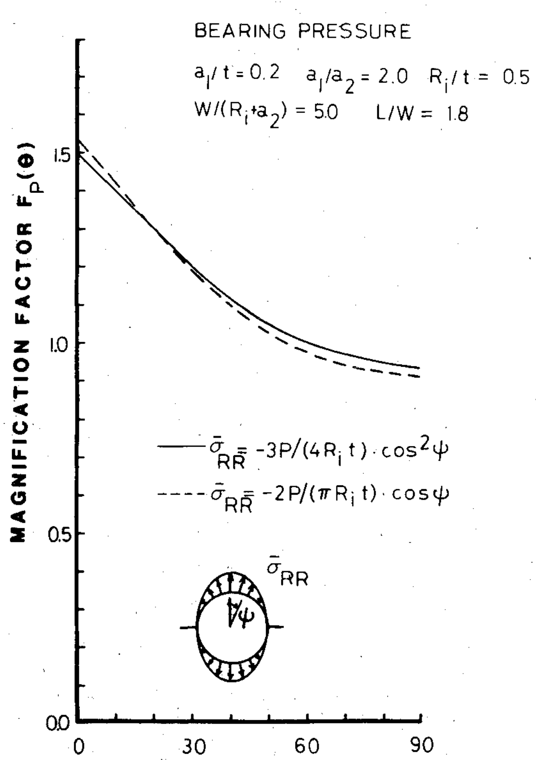

Fig. 10 Comparison of magnification factors with different types of bearing pressure loading.

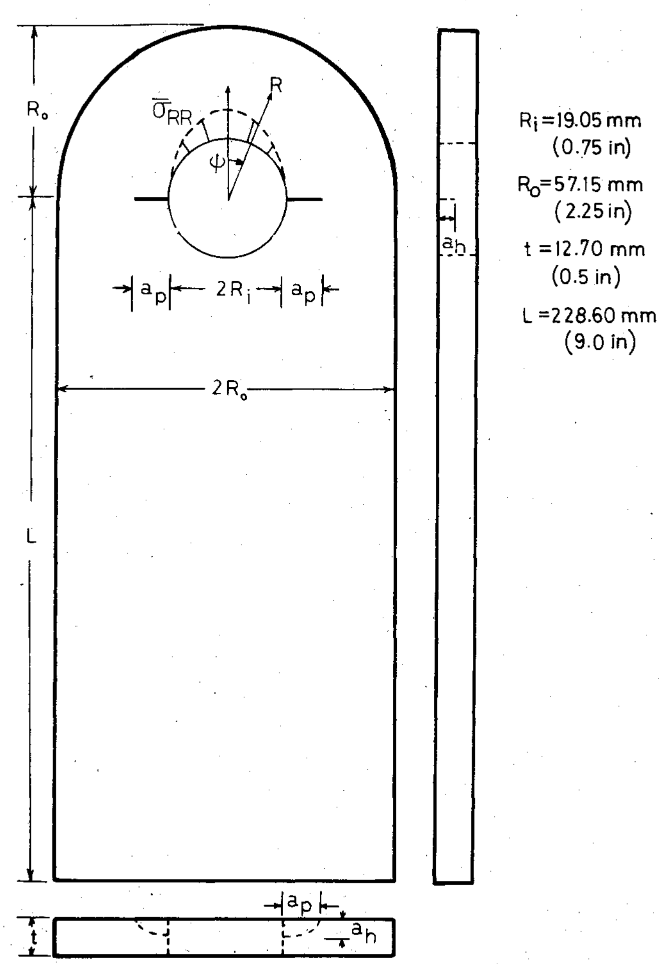

Fig. 11 Configuration of an attachment lug with two symmetric quarter-elliptical cracks emanating from the pin hole.

a formula developed by Shah,[24]

$$(K_I)_{\substack{\text{single}\\\text{crack}}} = \sqrt{\left(2R_it + \frac{\pi a_1 a_2}{4}\right) \Big/ \left(2R_it + \frac{\pi a_1 a_2}{2}\right)} \cdot (K_I)_{\substack{\text{two}\\\text{cracks}}} \quad (22)$$

Quarter-Elliptical Corner Cracks in Aircraft Attachment Lugs

The geometry of the lug with two symmetric quarter-elliptical corner cracks is shown in Fig. 11. The lug material is 7075-76 aluminum with Young's modulus $E=71.71$ GPa (10.4×10^6 psi) and Poisson's ratio $\nu=0.33$. To simulate pin loading, the cosine bearing pressure defined by Eq. (21) acting on only a half of the boundary $-\pi/2\leq\psi\leq\pi/2$, as shown in Fig. 11, is considered. The analysis was made for nine crack geometries as follows

$$a_p/a_h = 0.5,\ 1.2,\ \text{and}\ 2.0$$

$$a_h/t = 0.2,\ 0.5,\ \text{and}\ 0.8$$

where a_p and a_h denote crack lengths at the surfaces of the plate and hole, respectively. Thus, $a_p=a_2$ and $a_h=a_1$ for $a_p/a_h=0.5$, and $a_p=a_1$ and $a_h=a_2$ for $a_p/a_h=1.2$ and 2.0.

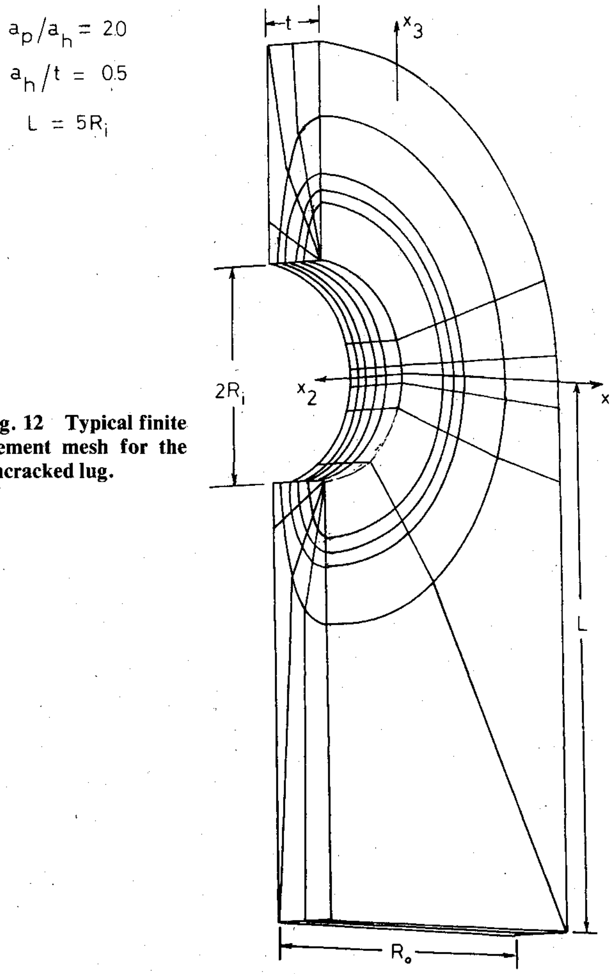

Fig. 12 Typical finite element mesh for the uncracked lug.

The typical finite element model used for the uncracked lug is shown in Fig. 12. This model consists of 140 twenty-noded isoparametric elements with 2250 degrees of freedom (before imposition of the boundary condition). Due to the symmetry a half of the lug was used in the analysis. The displacements were imposed as $u_3=0$ at $x_3=-L$, and $u_1=0$ at $x_1=-R_i$. The matrices $[G]_m$ were calculated on the surface of $x_2=0$, t, $R=R_0$ ($x_3\geq0$), and $x_1=R_0-R_i$ ($x_3<0$) satisfying Eq. (17), $r_{\min}<5a_1$ (see Fig. 12).

First, only stress analyses of the uncracked lug shown in Fig. 12 were performed to examine the effect of the lug length, changing $L=5R_i$ to $6R_i$. The average value of normal stress σ_{33} at the original crack location differs only 0.02% as the lug length changes from $5R_i$ to $6R_i$. Thus, the following analyses were done with $L=5R_i$. In addition, the magnitude of shear stresses which produce the stress intensity factors of modes II and III was also examined. The average values of the shear stresses σ_{31} and σ_{32} were, respectively, 0.5 and 0.1% of the normal stress σ_{33}. Thus the mode I stress intensity factor is dominant and the other modes are negligible in this case.

To evaluate the magnification factors for this problem the reference stress was chosen as $\sigma_i=\sigma_p=P/2R_it$. The complete elliptic integral of second kind $E(k)$ in Eq. (19) is given by 1.2111 for $a_p/a_h=0.5$ and 2.0, and 1.4429 for $a_p/a_h=1.2$. Figure 13 shows the magnification factors as a function of the elliptical angle for the aspect ratios of $a_p/a_h=0.5$, 1.2, and 2.0. The elliptical angle is always measured from the hole surface in these cases. Figure 14 shows the magnification factors as a function of the crack length at the plate surface a_p for the crack depth of $a_h/t=0.2$, 0.5, and 0.8. The magnification factors increase as the crack length a_p decreases, due to the fact that the stress concentration exists around the pin hole.

The stress intensity factors for all the crack geometries are summarized in Table 1. The stress intensity factors were

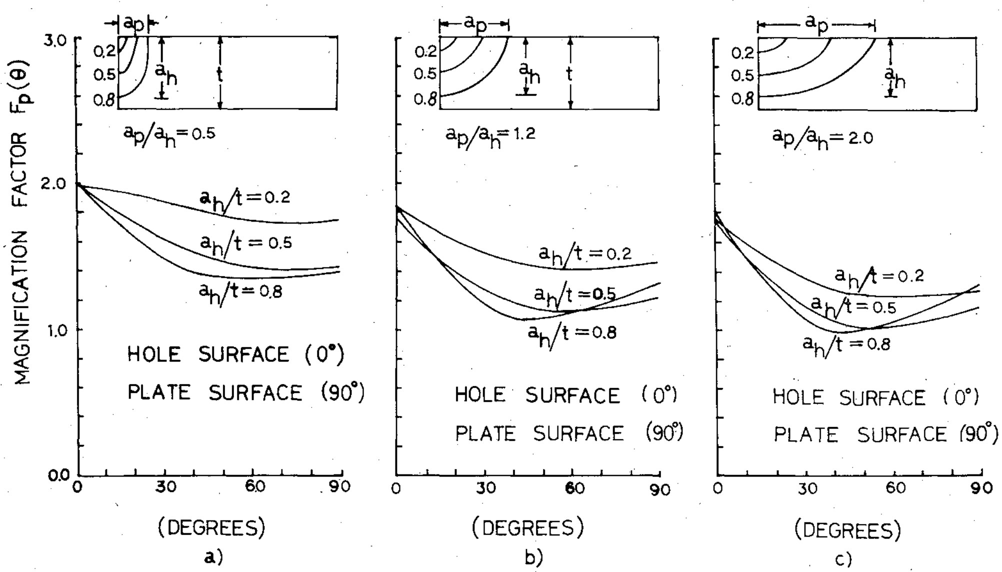

Fig. 13 Magnification factors vs the elliptical angle measured from the hole surface.

Table 1 Stress intensity factors ($K_I/\sigma_p\sqrt{\pi R_i}$) for quarter-elliptical corner cracks in an attachment lug

a_p/a_h	0.5			1.2			2.0		
Angle,[a] deg \ a_h/t	0.2	0.5	0.8	0.2	0.5	0.8	0.2	0.5	0.8
0	0.299	0.475	0.600	0.462	0.703	0.936	0.525	0.827	1.086
10	0.299	0.453	0.557	0.435	0.631	0.806	0.482	0.722	0.906
20	0.310	0.442	0.529	0.404	0.556	0.679	0.433	0.611	0.733
30	0.323	0.439	0.514	0.375	0.495	0.585	0.387	0.520	0.610
40	0.335	0.440	0.513	0.354	0.453	0.533	0.350	0.456	0.545
50	0.344	0.445	0.524	0.340	0.430	0.519	0.322	0.417	0.522
60	0.351	0.453	0.541	0.333	0.421	0.528	0.300	0.395	0.518
70	0.358	0.462	0.559	0.330	0.421	0.548	0.282	0.381	0.518
80	0.365	0.471	0.574	0.331	0.430	0.575	0.269	0.376	0.524
90	0.372	0.480	0.588	0.334	0.446	0.609	0.268	0.386	0.548

[a] The elliptical angle measured from the hole surface.

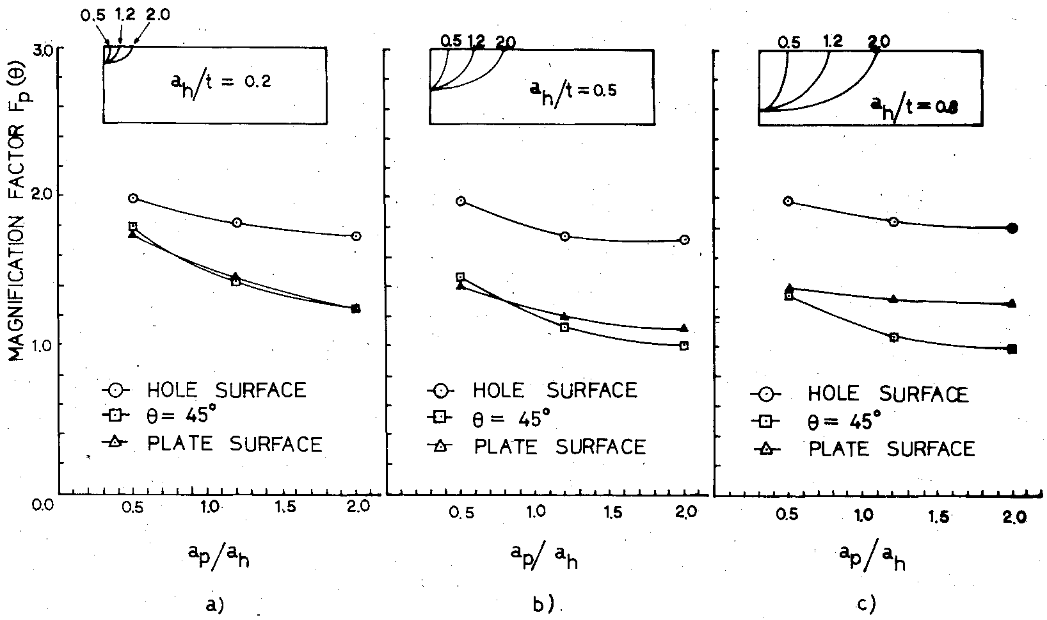

Fig. 14 Magnification factors vs crack aspect ratio.

normalized by the stress intensity factor for the crack size of $2R_i$ in an infinite two-dimensional plate with the pressure σ_p on the crack surface. As seen from Table 1 the stress intensity factor increases with the increasing size of the crack. The stress intensity factors for a single quarter-elliptical corner crack in the lug can also be approximated from the results for two symmetric corner cracks by using Eq. (22). The CPU time for the analyses was approximately 1800 s using the CYBER 74.

Conclusion

The alternating method, in conjunction with the finite element method and the complete, general analytical solution for an elliptical crack in an infinite solid, was developed for the analyses of quarter-elliptical corner cracks emanating a hole. The present finite element alternating method leads to at least an order of magnitude less expensive procedure for routine evaluation of accurate stress intensity factors in three-dimensional complex structural components, as compared to other techniques currently reported in literature.

Excellent correlation was found between the present solutions and those obtained by Raju and Newman[5,21] for a quarter-elliptical corner crack emanating a hole in the plate subject to remote tension as well as bearing pressure loading.

The stress intensity factors for various shapes of two symmetric quarter-elliptical corner cracks emanating the pin hole of aircraft attachment lugs were also determined by the present finite element alternating method. The stress intensity factors for a single corner crack can be approximated from the present solutions for two symmetric corner cracks by using Shah's conversion formula.[24]

It was also demonstrated in the present study that the stress intensity factor solution obtained by the alternating technique can be improved significantly when the degree of polynomials in the applied stress for the analytical solution is increased.

Acknowledgments

This work was supported by AFOSR under Grant 81-0057 to the Georgia Institute of Technology. The authors gratefully acknowledge this support as well as the encouragement received from Dr. A. Amos. The authors thank Ms. Margarete Eiteman for her careful assistance in the preparation of this manuscript.

References

[1] Lin, K. Y., Tong, P., and Orringer, O., "Effect of Shape and Size on Hybrid Crack-Containing Finite Elements," *Computational Fracture Mechanics,* edited by E. F. Rybicki and S. E. Benzley, ASME, New York, 1975, pp. 1-20.

[2] Liu, A. F. and Kan, P., "Test and Analysis of Cracked Lug," *Advances in Research on Strength and Fracture of Material,* Vol. 38, edited by D. M. R. Talpin, Pergamon Press, New York, 1977, pp. 657-664.

[3] Atluri, S. N. and Kathiresan, K., "Stress Analysis of Typical Flaws in Aerospace Structural Components Using Three-Dimensional Hybrid Displacement Finite Element Methods," *Proceedings of AIAA/ASME 19th Structural Dynamics and Materials Conference,* Bethesda, Md., Aug. 1978, pp. 340-350 (AIAA Paper 78-513).

[4]Hechmer, J. L. and Bloom, J. M., "Determination of Stress Intensity Factors for the Corner Cracked Hole Using the Isoparametric Singularity Element," *International Journal of Fracture,* Vol. 13, 1977, pp. 732-735.

[5]Raju, I. S. and Newman, J. C. Jr., "Stress-Intensity Factors for Two Symmetric Corner Cracks," *Fracture Mechanics,* edited by C. W. Smith, ASTM STP 677, 1979, pp. 411-430.

[6]Smith, F. W. and Kullgren, T. E., "Theoretical and Experimental Analysis of Surface Cracks Emanating from Fastener Holes," AFFDL-TR-76-104, Feb. 1977.

[7]Shah, R. C. and Kobayashi, A. S., "Stress Intensity Factor for an Elliptical Crack Under Arbitrary Normal Loading," *Engineering Fracture Mechanics,* Vol. 3, 1971, pp. 71-96.

[8]Heliot, J., Labbens, R., Pellissier-Tanon, A., "Application of the Boundary Integral Equation Method to Three-Dimensional Crack Problems," Paper 80-C2/PVP-119, presented at ASME Century Two Pressure Vessels & Piping Conference, San Francisco, Aug. 1980.

[9]McGowan, J. J. (ed.), "A Critical Evaluation of Numerical Solutions to the 'Benchmark' Surface Problem," *SESA Monograph,* 1980.

[10]Atluri, S. N. and Kathiresan, K., "Three-Dimensional Analysis of Surface Flaws in Thick Walled Reactor Pressure Vessels Using Displacement-Hybrid Finite Element Methods," *Nuclear Engineering and Design,* Vol. 51, No. 2, 1979, pp. 163-176.

[11]Atluri, S. N. and Kathiresan, K., "Stress Intensity Factor Solutions for Arbitrary Shaped Surface Flaws in Reactor Pressure Vessel Nozzle Corners," *International Journal of Pressure Vessels and Piping,* Vol. 8, 1980, pp. 313-332.

[12]Shah, R. C. and Kobayashi, A. S., "On The Surface Flaw Problem," *The Surface Crack: Physical Problems and Computational Solutions,* edited by J. L. Swedlow, ASME, New York, 1972, pp. 79-124.

[13]Kobayashi, A. S., Enetanya, A. N., and Shah, R. C., "Stress Intensity Factors of Elliptical Cracks," *Prospects of Fracture Mechanics,* edited by G. C. Sih, H. C. Van Elst, and D. Brock, Noordhoff International, Leyden, the Netherlands, 1975, pp. 525-544.

[14]Nishioka, T. and Atluri, S. N., "A Major Development Towards a Cost-Effective Alternating Method for Fracture Analysis of Steel Reactor Pressure Vessels," *Transactions of the 6th International Conference on Structural Mechanics in Reactor Technology,* Paper G1/2, Paris, 1981.

[15]Nishioka, T. and Atluri, S. N., "Analytical Solution for Embedded Elliptical Cracks, and Finite Element Alternating Method for Elliptical Surface Cracks, Subjected to Arbitrary Loadings," *Engineering Fracture Mechanics,* Vol. 17, No. 3, 1983, pp. 247-268.

[16]Vijayakumar, K. and Atluri, S. N., "An Embedded Elliptical Flaw in an Infinite Solid Subject to Arbitrary Crack-Face Tractions," *Journal of Applied Mechanics,* Vol. 48, 1981, pp. 88-96.

[17]Mondkar, D. P. and Powell, G. H., "Large Capacity Equation Solver for Structural Analysis," *Computers and Structures,* Vol. 4, 1974, pp. 699-728.

[18]Nishioka, T. and Atluri, S. N., "Analysis of Surface Flaws in Pressure Vessels by a New 3-Dimensional Alternating Method," *Aspect of Fracture Mechanics in Pressure Vessels and Piping,* ASME PVP Vol. 58, 1982, pp. 17-35.

[19]Hammer, P. C. and Stroud, A. H., "Numerical Evaluation of Multiple Integrals II," *Mathematical Tables and Other Aids to Computation,* Vol. XII, No. 61-64, 1958, pp. 272-280.

[20]Punch, E. F., Private communication, Georgia Institute of Technology, 1981.

[21]Newman, J. C. Jr. and Raju, I. S., "Stress-Intensity Factor Equations for Cracks in Three-Dimensional Finite Bodies," Paper presented at ASTM 14th National Symposium on Fracture Mechanics, Los Angeles, June 30-July 2, 1981.

[22]Nishioka, T. and Atluri, S. N., "Integrity Analysis of Surface-Flawed Aircraft Attachment Lugs: A New, Inexpensive 3-D Alternating Method," *Proceedings of AIAA/ASCE/ASME/AHS 23rd Structural Dynamics and Materials Conference,* New Orleans, May 1982, pp. 287-300 (Paper 82-0742).

[23]Newman, J. C. Jr., Private communication to S. N. Atluri, June 1982.

[24]Shah, R. C., "Stress Intensity Factors for Through and Part-Through Cracks Originating at Fastener Holes," *Mechanics of Crack Growth,* ASTM STP590, 1976, pp. 429-459.

[25]Brebbia, C. A., *The Boundary Element Method for Engineers,* John Wiley & Sons, New York, 1978.